Chapter 2
Longitudinal Flow Field

Abstract The state of the science in predicting the hydrodynamically developed longitudinal field of non-linear viscoelastic fluids in straight tubes of arbitrary but longitudinally constant cross section and in predicting the friction factors is summarized. Laminar and turbulent longitudinal flow fields and related phenomena including recent progress concerning the all-important drag reduction phenomena are addressed.

Keywords Non-linear viscoelastic fluids • Longitudinal velocity field • Straight tubes • Arbitrary cross-section • Friction factors • Laminar flow • Turbulent flow • Pseudoplastic behavior • Drag reduction • Drag-reducing additives and applications • Theoretical mechanism of drag reduction • Experimental findings in drag reduction • Factors influencing the effectiveness of drag reduction

Only hydrodynamically developed flows will be reviewed. It should be noted that hydrodynamically developing flows are important as the entrance length L given in terms of either dimensionless quantities L^+ or L^*,

$$L = L^+ D_h Re^+, \qquad L = L^* D_h Re^*,$$

can be substantial in particular in laminar flow. Here D_h is the hydraulic diameter, and Re^+ and Re^* are the generalized Reynolds number and the Kozicki generalized Reynolds number, respectively, defined in Sect. 2.1.

2.1 Laminar Flow

The comprehensive monograph by Shah and London [1] which covers the research up to 1978 with an extensive bibliography and the review by Shah and Bhatti [2] which appeared a decade later are excellent references for the calculation of the friction factors f for Newtonian fluids in fully established laminar flow in ducts of non-circular shape. The investigations by Eckert and Irvine [3] and Carlson and Irvine [4] on the pressure drop in triangular-shaped ducts are among the earliest on the friction factor in fully established flow of Newtonian fluids in tubes of non-circular

D.A. Siginer, *Developments in the Flow of Complex Fluids in Tubes*,
DOI 10.1007/978-3-319-02426-4_2

cross sections. For the much emphasized rectangular cross sections, Shah and London [1] provide an approximate formula

$$fRe = 24\left(1 - 1.355\alpha^* + 1.9467\alpha^{*2} - 1.7012\alpha^{*3} + 0.9564\alpha^{*4} - 0.2537\alpha^{*5}\right) \tag{2.1}$$

where the Reynolds number Re is based on the hydraulic diameter D_h and α^* represents the duct aspect ratio with height $2b$ over width $2a$. The approximate formula (2.1) stays within 0.05 % of the correct analytical solution. A simpler but a slightly more approximate formula valid when $\alpha^* \geq 0.05$ whose predictions stay within 0.25 % of those based on the exact analytical velocity w profile,

$$w = \frac{16a^2}{\pi^3\eta}\left(-\frac{\mathrm{d}p}{\mathrm{d}z}\right)\sum_{k=1}^{\infty}\left(\left[\frac{(-1)^{k-1}}{(2k-1)^3}\right]\left\{1 - \frac{\cosh\left[(2k-1)\frac{\pi y}{2a}\right]}{\cosh\left[(2k-1)\frac{\pi b}{2a}\right]}\right\}\cos\frac{(2k-1)\pi x}{2a}\right),$$

was obtained by Natarajan and Lakshmanan [5],

$$fRe = 14.4(\alpha^*)^{-1/6}.$$

In these formulas the pressure, the viscosity, and the longitudinal coordinate are denoted by p, η, and z, respectively. The friction factors for the fully developed laminar flow of power-law fluids in rectangular channels were calculated by Schecter [6] and Wheeler and Wissler [7] via a variational method and a numerical solution, respectively. The latter authors derive an approximate equation for the square duct geometry,

$$4fRe^+ = 7.4942\left\{\frac{1.7330}{n} + 5.8606\right\}^n$$

$$Re^+ = \frac{\rho\overline{w}^{2n}D_h^n}{K}.$$

where $\overline{w}$ is the average velocity. In fully established laminar flow in circular tubes, the pressure drop of power-law fluids was predicted based on the constitutive assumption, Metzner and Reed [8],

$$\tau = K\left(2tr\mathbf{D}^2\right)^{\frac{n}{2}} \tag{2.2}$$

where τ and $\mathbf{D}$ represent the shear stress and the rate of deformation tensor with K and n referring to the consistency and the power index, respectively. The solution of the momentum equation for the longitudinal flow velocity w with the constitutive assumption Eq. (2.2) gives for the fully established velocity profile w,

$$\frac{w}{w_{\max}} = \frac{3n+1}{n+1}\left\{1 - \left[\frac{r}{R}\right]^{\frac{n+1}{n}}\right\}$$

with $w_{\max}$ and R standing for the maximum velocity and the circular tube radius. The friction factor f is defined in terms of a generalized Reynolds number Re',

$$f = \frac{16}{Re'}$$
$$Re' = \rho(w_{\max})^{2-n}(2R)^n\left\{8^{n-1}K\left[\frac{3n+1}{4n}\right]^n\right\}^{-1} \tag{2.3}$$

That this prediction for purely viscous (generalized Newtonian) fluids also holds for viscoelastic fluids in circular pipes was shown by Metzner [9] and Cho and Hartnett [10]. The flow of a generalized Newtonian fluid in ducts of arbitrary cross section was investigated by Kozicki et al. [11] via a generalized Rabinowitsch–Mooney approach. They show in particular that the friction factor for the fully established laminar flow of a power-law fluid in rectangular geometries is given with good accuracy by

$$f = \frac{16}{Re^*},$$
$$Re^* = \rho(w_{\max})^{2-n}D_h^n\left\{8^{n-1}K\left[F(b) + \frac{F(a)}{n}\right]^n\right\}^{-1} \tag{2.4}$$

where $F(b)$ and $F(a)$ are functions of the geometry of the tube, that is, of its aspect ratio α^*, and are tabulated. For instance, for an aspect ratio of $\alpha^* = 0.5$, the values assumed by $F(a)$ and $F(b)$ are 0.2439 and 0.7278, respectively. If $F(a)$ and $F(b)$ are assigned the values of 0.25 and 0.75, respectively, circular duct is obtained and Eq. (2.4) collapses onto Eq. (2.3).

That these predictions based on a purely viscous generalized Newtonian model also hold well for viscoelastic fluids with good accuracy, in particular in rectangular geometries, was proven by the experiments of Hartnett et al. [12], Hartnett and Kostic [13], and Bamidipaty [14] who investigated the flow in a square tube, in a tube of aspect ratio 2 (height is twice as large as the width), and in a tube of aspect ratio 5, respectively, to determine that the overall agreement with power-law predictions is within 10 %. It should be emphasized that given the unavoidable experimental scatter this is a very good agreement. There are no experimental pressure drop measurements available for the fully established laminar flow of viscoelastic fluids in arbitrary cross sections. But on the basis of the evidence available for rectangular cross sections, it makes sense to extend the findings for rectangular cross sections to arbitrary cross sections and assume that unless future experimental evidence proves the contrary pressure drop in the fully established

laminar flow of viscoelastic fluids in tubes of arbitrary but constant cross section in the longitudinal direction is well predicted by the generalized Newtonian model.

However, recent research by Siginer and Letelier [15] provides evidence that elastic effects clearly contribute to the longitudinal velocity field, and thus predicting the longitudinal velocity field with power-law type of constitutive equations that does not account for elastic effects, reasonably good that the predictions may be, would give only approximately correct results. Siginer and Letelier [15] have studied the fully developed steady pressure-gradient-driven laminar flow of a class of non-linear and non-affine, single mode, quasilinear viscoelastic fluids with instantaneous elasticity in straight tubes of arbitrary cross section. The class of viscoelastic fluids investigated includes the non-affine Johnson–Segalman [16] and Phan-Thien [18] models and the affine Phan-Thien–Tanner [17] model as special cases (see Sect. 3.6.1 for details). A continuous one-to-one mapping is used to obtain arbitrary tube contours from a base tube contour ∂D_o, Siginer and Letelier [15]. The analytical method presented is capable of predicting the velocity field in tubes with arbitrary cross section. The base flow is the Newtonian field and is obtained at $O(1)$. Field variables are expanded in asymptotic series in terms of the Weissenberg number We. The analysis does not place any restrictions on the smallness of the driving pressure gradients which can be large and applies to dilute and weakly elastic non-linear viscoelastic fluids. The Newtonian field in arbitrary contours is obtained, and longitudinal velocity field components due to shear thinning and to non-linear viscoelastic effects are identified. Third-order analysis shows a further contribution to the longitudinal field driven by first normal stress differences. Their analysis provides evidence that predicting the longitudinal velocity field of non-linear viscoelastic fluids in straight tubes with power-law type of constitutive equations that does not account for elastic effects is only approximate, reasonably good that it may be, for elastic effects clearly contribute to the longitudinal velocity field. Their research, on secondary flows in arbitrary cross-sectional tubes driven by unbalanced second normal stresses in the cross section, is summarized in Sect. 3.6.1. Longitudinal equal velocity contours, the first and the second normal stress differences, as well as wall shear stress variations are discussed for several non-circular contours some for the first time. Examples are shown in Figs. 2.1 and 2.2.

A numerical method to predict the longitudinal velocity field based on the mapping of the simply connected physical flow domain of a straight tube of arbitrary cross section onto a circular computational domain and the efficient and robust Levenberg–Marquardt algorithm, Chai and Yeow [19], has been devised by Ahmeda et al. [20]. The approach they develop permits simple discretization schemes in the circular computational domain leading to simultaneous determination of the velocity and stress contours. The method is applied to the flow of Newtonian, purely viscous non-Newtonian inelastic as well as viscoelastic fluids of the memory integral viscoelastic K-BKZ (Kaye–Bernstein–Kearsley–Zapas) type. Their results show that the shear stress and the velocity in an arbitrary cross section, specifically a square cross section, corresponding to the constitutive equation of the purely viscous type (Eq. 2.5a) and corresponding to the viscoelastic fluid

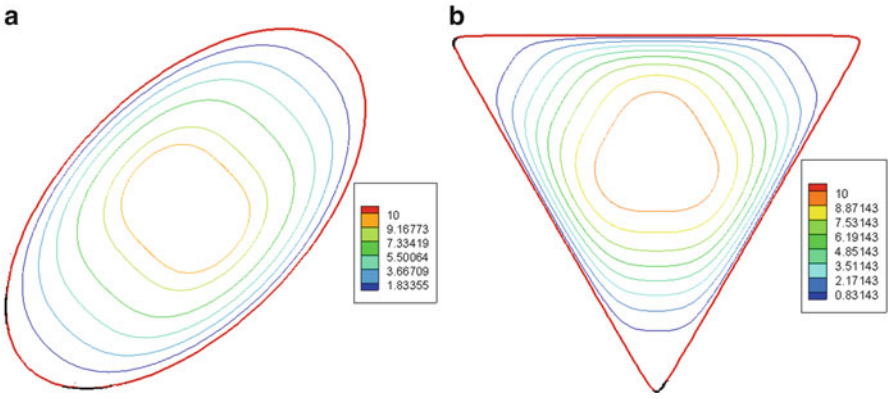

Fig. 2.1 Velocity level lines in an (**a**) elliptical contour ($n = 2$, $\varepsilon = 0.4$) and in a (**b**) triangular cross section ($n = 3$, $\varepsilon = 0.384$): $Re = 200$, $We = 0.3$, $\xi = 0.3$. (n, ε) represent mapping parameters and Re, We and ξ stand for the Reynolds number, the Weissenberg number and the non-affine slippage constant, respectively. See Sect. 3.2 for a definition of the Weissenberg number and the slippage constant (reprinted from Siginer and Letelier [15] with permission)

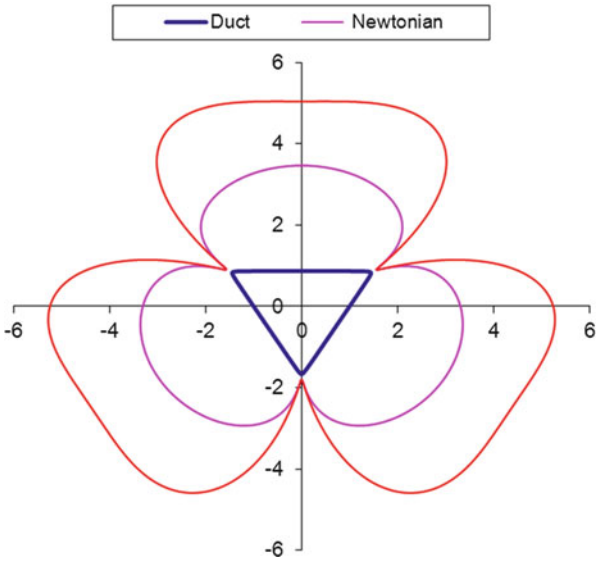

Fig. 2.2 Normalized wall shear stress τ_0 for Newtonian and viscoelastic fluids in a triangular duct $Re = 200$: (**a**) Newtonian, (**b**) viscoelastic: $We = 0.3$, $\xi = 0.2$ (reprinted from Siginer and Letelier [15] with permission)

(Eq. 2.6) of the K-BKZ type, the Papanastasiou model [21] of the same zero shear viscosity μ_0, are quite different, thereby affirming that elasticity plays a significant role in determining the longitudinal flow field along the lines of the findings of Siginer and Letelier [15].

$$\mathbf{T} = -p\mathbf{1} + 2\eta(\mathbf{D})\mathbf{D} \tag{2.5a}$$

$$\eta(\mathbf{D}) = \eta_0 \left[1 + \left(\dot{\gamma}\,\eta_0/\lambda\right)^a\right]^{-b} \tag{2.5b}$$

$$\mathbf{T}(t) = -p\mathbf{1} + \int_{-\infty}^{t} \Psi\left(\mathrm{I}_{\mathbf{C}^{-1}}, \mathrm{II}_{\mathbf{C}^{-1}}\right) \sum \frac{a_k}{\lambda_k} e^{-(t-\tau)/\lambda_k} \mathbf{C}_t^{-1}(\tau)\mathrm{d}\tau \tag{2.6}$$

In the above $\mathbf{T}$, p, $\mathbf{1}$, η, $\dot{\gamma}$, λ, Ψ, a and b represent the total stress tensor, the constitutively indeterminate part of the stress, the unit tensor, the shear rate dependent viscosity, the shear rate, the relaxation time, and a kinematic function of the first and second invariants $\mathrm{I}_{\mathbf{C}^{-1}}$ and $\mathrm{II}_{\mathbf{C}^{-1}}$ of the Finger tensor $\mathbf{C}_t^{-1}$, respectively. a and b in Eq. (2.5b) are curve fitting constants to be determined from experiments, and a_k and λ_k in Eq. (2.6) are the relaxation moduli and the relaxation times of the fluid.

The work of Siginer and Letelier [15] as well as of Ahmeda et al. [20] clearly demonstrates the effect of elasticity in computing the longitudinal field and the related components of the stress tensor. The conjecture that the longitudinal fields of viscoelastic fluids and purely viscous fluids of the power-law type are one and the same in tubes of arbitrary cross sections and can be predicted with good accuracy, if a modified Reynolds number of the Kozicki (Eq. $2.4)_2$ type is used, flows out of experimental measurements for rectangular cross sections which do show a 10 % difference from the predictions if the fluid is viscoelastic. But this much difference is in pace with the calculations of Siginer and Letelier [15] for arbitrary cross sections, that is, the influence of the fluid elasticity on the longitudinal field is of the order of 10 %. The fact that the use of the Kozicki Reynolds number may yield good results for viscoelastic fluids in rectangular cross sections may be due to a large extent to the empirical/phenomenological cross section-dependent constants $F(a)$ and $F(b)$ built in Eq. (2.4).

2.2 Turbulent Flow

An extensive review of the analytical and experimental studies for friction factor of Newtonian fluids for turbulent flow in non-circular ducts can be found in Bhatti and Shah [22].

2.2.1 Viscoelastic Fluids: Pseudoplastic Behavior

Predictions of the pressure drop of linear fluids in turbulent flow based on the assumption that the universal turbulent velocity profile in circular ducts is also valid for non-circular tubes are not accurate. This assumption is prompted by the observation that most of the momentum change in turbulent flow occurs in the laminar sublayer near the wall, and the velocity profile is relatively flat over the rest of the

cross section. Hartnett et al. [23] found that experimental measurements with rectangular ducts of various aspect ratios are always larger than the predicted values with the square duct representing the worst case of departure; at Reynolds numbers higher than 10^4, the magnitude of the departure is about 12 % higher. The physical explanation lies with the secondary flow which accompanies the turbulent flow of linear fluids in non-circular ducts. Secondary flows provide a mechanism for the continuous transport of momentum from the central region of the tube toward the walls and in particular the corners thereby enhancing the velocity magnitudes there.

The fully developed turbulent friction factor for linear fluids flowing in rectangular cross sections and annuli can be predicted by formulas proposed by Jones [24] based on correlations of available experimental data. For instance, the friction factor f for rectangular ducts is given by

$$\frac{1}{\sqrt{f}} = 4.0 \log\left(Re_N^* \sqrt{f}\right) - 0.4,$$

$$Re_N^* = Re\,\Phi(\alpha^*), \qquad \Phi(\alpha^*) = \frac{1}{F(a) + F(b)}$$

where the Re is based on the hydraulic diameter D_h and $F(a)$ and $F(b)$ are the same tabulated functions which appear in Eq. (2.6). $\Phi(\alpha^*)$ can also be computed from an exact

$$\Phi(\alpha^*) = \frac{2(1+\alpha^*)^2}{3}\left\{1 - \frac{192}{\pi^5}\alpha^* \sum_{k=0}^{\infty} (2k+1)^{-5} \tanh\frac{(2k+1)\pi}{2\alpha^*}\right\},$$

or an approximate formula, accurate to 2 %,

$$\Phi(\alpha^*) = \frac{2}{3} + \frac{1}{8}\alpha^*(2 - \alpha^*).$$

A formula to determine the friction factor in the fully developed turbulent flow of generalized Newtonian fluids in circular pipes was proposed by Dodge and Metzner [25],

$$\frac{1}{\sqrt{f}} = \frac{4.0}{n^{0.75}} \log\left\{Re\, f^{\frac{(2-n)}{2}}\right\} - \frac{0.4}{n^{1.2}}. \tag{2.7}$$

The functional coefficients $\frac{4.0}{n^{0.75}}$ and $\frac{0.4}{n^{1.2}}$ in this equation are determined from correlations of experimental measurements of the pressure drop of aqueous Carbopol solutions and slurries of clay (Attagel) in the range $0.3 < n < 1$ for the power-law index. Rheological measurements taken on oscillatory rheometers clearly demonstrate that these are viscoelastic fluids, and yet they behave as purely viscous, that is, pseudoplastic fluids in turbulent flow in circular pipes without generating a drag-reducing effect. Dodge and Metzner [25] also proposed a

universal velocity profile for generalized Newtonian fluids in turbulent tube flow divided into a laminar sublayer, a buffer layer, and a turbulent core region similar in overall structure to the Newtonian Karman–Nikuradse three-layer model where the interface between the buffer layer and the turbulent core region is at $y_2 = y_2^+$. The superscript $^+$indicates dimensionless entities represented in terms of wall coordinates normalized by the friction velocity $u\tau = \sqrt{\tau w/\rho}$ and kinematic viscosity ν, where τw is the shear stress at the wall and ρ is the fluid density.

$$u^+ = \left\{ \begin{array}{lll} (y^+)^{1/n} & y^+ < 5^n & \text{laminar sublayer} \\ \frac{5.0}{n}\ln y^+ - 3.05 & 5^n < y^+ < y_2^+ & \text{buffer layer} \\ \frac{2.78}{n}\ln y^+ + \frac{3.8}{n} & y_2^+ < y^+ & \text{turbulent core} \end{array} \right\},$$

As early as 1966 Kozicki et al. [26] suggested that the Dodge–Metzner equation (2.7) can be used to predict the pressure drop in turbulent flow in tubes of arbitrary cross section by substituting the hydraulic diameter for the pipe diameter. This suggestion was further modified by Kostic and Hartnett [27] who proposed to use Eq. (2.7) replacing *Re* with the Kozicki Reynolds number *Re** defined in Eq. (2.4). The validity of this approach was proven by Hartnett et al. [12] and Hartnett and Rao [28] who conducted experiments with Carbopol and Attagel solutions in square and rectangular ducts, respectively, for a wide range of power-law index values and for Kozicki Reynolds numbers in the range of $3{,}000 < Re^* < 50{,}000$.

2.2.2 Drag-Reducing Viscoelastic Fluids

2.2.2.1 Preliminaries

As it was pointed out in the previous paragraph, not all viscoelastic fluids are of the drag-reducing type. Carbopol solutions and Attagel clay slurries fall in that category, and their pressure drop in turbulent flows can be predicted following the guidelines outlined in the previous paragraph. However, the class of drag-reducing viscoelastic fluids such as those obtained by dissolving small amounts of long chain polymers in water or in another solvent behaves quite differently. Examples are polyacrylamide, Separan, polyethylene oxide, carboxymethylcellulose (CMC), and hydroxyethylcellulose (Natrosol). Reductions of more than 30 % in the frictional drag were observed with additive concentrations of less than 50 parts per million by weight (wppm). At very small concentrations of the order of 10 wppm, the measured apparent viscosity of these fluids does not show any deviation from the Newtonian viscosity, but the observed experimental friction factors are significantly lower than the Newtonian values. An increase in the concentration produces an increase in the apparent viscosity and in the characteristic relaxation time of the fluid accompanied by a corresponding decrease in the friction factor. The friction factor decreases with

increasing concentration reaching an asymptotic value. Further increases in the concentration do not produce further decreases in the friction factor. This asymptotic behavior was first reported by Virk and his colleagues [29–31] who developed a comprehensive theory and correlation of drag-reducing activity based on their own work with pipe flow of polyethylene oxide solutions consistent with data obtained with other aqueous polymer solutions. It is interesting to note that pipe wall roughness is not a factor in drag reduction. Virk [32] reported that the onset of drag reduction in rough pipes occurred at the same wall shear stress as in smooth pipes, and the onset wall shear stress was essentially independent of polymer concentration and was unaffected by the flow regime (hydraulically smooth, transitional, or fully rough) during which onset occurs. The maximum drag reduction possible in the rough pipes was limited by an asymptote which was independent of polymeric parameters. Under asymptotic conditions, friction factors in all rough pipes identically obeyed the smooth pipe friction factor relation. Interestingly the maximum viscous sublayer thickness attained during drag reduction was approximately 2½ times that of Newtonian sublayer.

Experimental evidence is convincing that the extent of drag reduction is limited by a unique asymptote. The minimum drag asymptote in a circular geometry can be expressed both in implicit and explicit form, Virk et al. [31],

$$\frac{1}{\sqrt{f}} = 19.0 \log_{10}\left(Re\sqrt{f}\right) - 32.4,$$

$$f = 0.59\, Re^{-0.58}.$$

The latter expression for the asymptote is valid in the region $4 \times 10^3 \leq Re \leq 4 \times 10^4$. A slightly lower asymptote expressed in terms of the Reynolds number based on the apparent viscosity at the wall and which shows good agreement with experimental data in square and rectangular ducts has been proposed by Cho and Hartnett [13],

$$f = 0.2\, Re^{-0.48}.$$

The behavior of polyacrylamide solutions in water in circular pipes has been studied by Hartnett and Kwack [33]. They establish that the friction factor in turbulent flow for these fluids is a function of the Re and We numbers below a critical $We_{\mathrm{cr}} \sim 10$. For Weissenberg numbers We below this value the friction factor decreases with increasing We at a fixed Re reaching an asymptotic value at a $We \sim 10$. Beyond the critical value $We_{cr} = 10$, friction factor in fully established flow is a function of the Re only. The experiments were conducted in the range $10^4 < Re < 7 \times 10^4$. The critical Weissenberg number We_{cr} is not fixed for all Re and increases with increasing Re; for $Re = 10^4$ the value of $We_{cr} \sim 7$, whereas for $Re = 7 \times 10^4$ it assumes a numerical value larger than 10 about $We_{cr} \sim 11$. The same conclusions were reached by Ghajar and Azar [34] who experimented with other aqueous polymeric solutions, two different types of Separan. At a fixed Re for values of $We > We_{cr}$, the friction factor f is a constant. A critical We_{cr} is reached

with decreasing We at a fixed Re. The friction factor increases with decreasing We for values of $We < We_{cr}$ gradually approaching the Newtonian value as the We approaches zero (see Sect. 3.5.2 for more on this topic).

2.2.2.2 Drag-Reducing Additives and Applications

Experimental pressure drop data for the turbulent flow of drag-reducing fluids in non-circular geometries are relatively rare in the literature with the exception of rectangular ducts. However, on the basis of the available evidence with rectangular tubes, the above results valid for circular cross sections can be cautiously extended to arbitrary non-circular geometries subject to future experimental verification. A very promising novel experimental technique based on nuclear magnetic resonance imaging (NMR) dubbed Rheo-NMR has been recently introduced, Schroeder and Jeffrey [35]. The real-time, non-invasive system does not require discreet tracers and allows the resolution of all velocity components, longitudinal and transversal, with equal ease. The technique has been known for some time going as far back as 1991 Callaghan [36]; however, its application to non-Newtonian flows occurred only recently.

The phenomenon of drag reduction, the dramatic decrease in pressure drop or equivalently the substantial reduction in the friction factor in turbulent tube flow when a minute amount of a high molecular weight polymer is added to a Newtonian fluid, thereby reducing wall shear stresses, was discovered by Toms [37] in 1948. However the first *recognized* drag reduction result is due to Mysels [38] who had determined earlier that the skin friction for gasoline in pipe flow was significantly reduced by the addition of an anionic surfactant. The process was patented by Mysels [39] in 1949. Since then, it has been found that many other types of additives, including wormy micelle-forming surfactants, bubbles, rigid fibers, and even solid spheres, lead to drag reduction in turbulent flow. Natural fibers such as wood pulp are preferable because they have a "low environmental load" and other advantages such as lack of degradation of the solution as polymeric additives do over time. Reduced energy loss in the turbulent pipe flow of wood pulp fiber suspensions in water was reported for the first time by Forrest and Grierson [40]. But their paper did not receive the attention it deserved and it went unnoticed. Synthetic fibers have the same advantage as natural fibers in terms of "degradation," but they require careful disposal as by their very nature they are chemicals and may contaminate rivers and soil when solutions are drained directly, very much like polymeric and surfactant solutions. Kubo and Ogata [41] recently suggested the use of bamboo fibers as drag-reducing agents. Wood pulp fibers produce a 20 % in energy savings as a ballpark figure at $Re \sim 2 \times 10^4$. Bamboo fibers generate the same energy savings, but cleared woods take much longer than bamboos to regenerate, thus the environmental advantage. Although fibers are chemically and mechanically stable in an aqueous environment, the use of fibers comes with a serious drawback as any type of fiber can cause plugging problems in pipelines due to the high concentration of fibers, as high as a few percent, required for drag reduction.

The applications in energy savings are widespread with intense research efforts in reducing energy losses in pipelines, drag reduction over ship and submarine hulls, and improving efficiency of district heating and cooling systems, in which chilled or heated water is generated at a central location in a city and pumped to buildings in the surrounding area. Drag-reducing additives greatly decrease system energy requirements, reducing pipe diameter or increasing flow rate. The first application of drag-reducing additive was in transport of crude oil in the Trans-Alaska (TAPS or Alyeska) Pipeline in 1979. The pipeline is 800 miles long with 48 in. diameter. Injecting a concentrated solution of a high molecular weight polymer downstream of pumping stations at homogeneous concentrations as low as 1 ppm increased crude throughput by up to 30 %, Burger et al. [42]. District heating or cooling systems provide or remove heat in buildings or a district by recirculating water heated or chilled at a central station. The water recirculation energy requirements make up about 15 % of the total energy for a district heating or cooling system. Surfactants can reduce pumping energy requirements by 50–70 %. The effectiveness depends on the kinds of additives used and the layout of the primary distribution system. Surfactant drag-reducing additives have been tested successfully in large-scale district heating systems in Denmark, Germany, and the Czech Republic and in district cooling systems in Japan with very significant savings in energy requirements. For instance, cationic surfactants in aqueous systems have been used in over 130 buildings throughout Japan and reduced pumping energy by 20–60 %. A novel application of surfactants is preventing flow-induced localized corrosion. Repeated impact of turbulent eddies on the wall causes intermittent stresses on the wall leading to mechanical damage to the surface material. Surfactants successfully suppress the formation of turbulent eddies near the wall.

2.2.3 The Mechanism of Drag Reduction

2.2.3.1 Experimental Findings

Experimental flow visualization techniques were developed in the late 1960s to probe and resolve the structure of the boundary layer in turbulent flows of homogeneous Newtonian fluids. The formation of low-speed streaks in the laminar sublayer in the region very near the wall and their interaction with the outer portions of the flow through a process of gradual lift-up, then sudden oscillation, bursting, and ejection into the main flow were discovered and investigated by Klein et al. [43]. Suspended solid colloidal size particles and high-speed motion picture camera moving with the flow were used by Corino and Brodkey [44] to investigate the viscous sublayer. They find that fluid elements are periodically ejected outward toward the centerline from a thin region adjacent to the sublayer. They identify a zone of high shear at the interface between the mean flow and the decelerated region that gives rise to the ejected elements. The interaction of the ejected

elements with the mean flow in this high-shear region creates intense, chaotic velocity fluctuations, which are believed to be an important factor in the generation and maintenance of turbulence. Electrochemical techniques were used to measure the circumferential component of the velocity gradient in turbulent flow at the wall of a pipe by Sirkar and Hanratty [45], and hydrogen-bubble and hot-wire measurements with dye visualization were employed by Kim et al. [46] to investigate the boundary layer structure on a smooth-surface flat plate in a low-speed water flow to show that essentially all turbulence production occurs during intermittent *bursting* periods.

These developments encouraged Eckelman et al. [47] to look into the effect of drag-reducing additives on the production of turbulence in the viscous sublayer. The expertise gained and the methods developed for homogeneous Newtonian fluids were applied to turbulent flow of drag-reducing fluids starting in the early 1970s to examine the modification of the wall layer by polymeric additives and the turbulence production mechanism in the sublayer in the presence of additives, Donohue et al. [48], Fortuna and Hanratty [49]. The data of the former authors taken in the near-wall region of a fully developed two-dimensional channel flow showed that the spatially averaged bursting rate of low-speed streaks characteristic of the viscous sublayer decreased substantially suggesting that the dilute polymer solution decreases the production of turbulent kinetic energy in the near-wall region by inhibiting the formation of low-speed streaks. The authors explain this behavior, however, tentatively but perhaps for the first time, by high resistance to elongational strains and vortex stretching. Fortuna and Hanratty [49] conducted experimental studies of the influence of drag-reducing polymers on the time-averaged velocity gradient and on the two components of the fluctuating velocity gradient at the wall and concluded that the increase in drag reduction is accompanied by an increase of the size of longitudinally oriented eddies in the viscous sublayer. They speculate that polymer additives act to increase the viscous resistance in the transverse direction more than in the direction of the mean flow. Measurements made on a drag-reducing polymer solution in pipe flow using a novel type of laser Doppler meter developed by the author himself were reported in Rudd [50] with the conclusion that the polymer has very little effect upon the turbulent core of the flow, but thickens and stabilizes the viscous sublayer with turbulent intensity inside the sublayer unchanged; due to the thickening of the sublayer velocity, fluctuations just outside of it are greater. Dye visualization and motion picture techniques were used by Oldaker and Tiederman [51] to obtain a detailed description of the streak formation in the viscous sublayer. They find that the average transverse spacing of the streaks increases as the amount of drag reduction increases. The average streak spacing within the viscous sublayer is not a function of the distance from the wall in water flows and flows at lower levels of drag reduction. At high levels of drag reduction, the average spacing varies within the sublayer increasing as the wall is approached. Real-time hologram interferometry was used for flow visualization and turbulence measurements in the near-wall region in the spanwise direction and the direction normal to the wall by Achia and Thompson [52] to investigate the streaks and bursts that originate in the sublayer. Their data suggests a stabilized wall layer

with less turbulence production. They also suggest the extensional viscosity of the dilute polymer solution as the most likely mechanism underlining this behavior. It was suggested by various researchers, among them Lumley [53] who argued that the buffer region is the area of importance in drag-reducing flows and that drag reduction can result if behavior in the sublayer and buffer layer differ. Reischman and Tiederman [54] examined this issue by taking velocity measurements in drag-reducing flows in a two-dimensional channel with a laser Doppler anemometer with solutions of polyacrylamide and polyethylene oxide producing drag reductions ranging from 24 to 41 %. They establish that the drag-reducing mean velocity profile can be divided into three zones: a viscous sublayer, a buffer or interactive region, and a logarithmic region. They find no evidence that the viscous sublayers of the drag-reducing channel flows are thicker than those in the solvent flows. In addition the normalized streamwise fluctuations are essentially the same in both the solvent and drag-reducing sublayers. They find that the changes caused by the polymer addition occur in the buffer region. The drag-reducing buffer region is thicker and the velocity profile in the outer flow region accommodates this buffer region thickening. The measurements of the streamwise velocity fluctuations also show that the polymer additives redistribute the primary turbulent activity over a broadened buffer region. The role of the linear sublayer and the buffer layer was further clarified by the experiments of Tiederman et al. [55] who determined that the presence of additives does not affect at all the spanwise spacing and bursting rate of the streaks in the linear sublayer, which stays the same as that of water by itself. But in the buffer zone, the dimensionless spanwise streak spacing increases and the average bursting rate decreases. The latter rate is larger than the former. Thus, the additives have a direct effect on the flow processes in the buffer region, and the linear sublayer appears to have a passive role in the interaction of the inner and outer portions of the turbulent wall layer. The work of McComb and Rabie [56, 57] is in general support of these findings as are the experimental results of Usui et al. [58]. The work of the latter authors, who measured turbulent characteristics of drag-reducing flow by laser Doppler velocimetry (LDV), suggests that polymer (aqueous solutions of polyethylene oxide) injection into a pipe flow caused a thickening of the buffer layer, enlargement of macroscale turbulent eddies, and suppression of fine-scale turbulent eddies. Luchik and Tiederman [59] reported that turbulence statistics are significantly modified even at very low concentrations of polymeric additive with approximately 30 % drag reduction at a concentration of 1–2 ppm. They also reported that the principal influence of the additives is to damp velocity fluctuations normal to the wall in the buffer region and that the average time between bursts increased for the drag-reducing flows as compared to the flow of water alone. The experiments of Walker and Tiederman [60] clarified the role of various terms in the Reynolds stress transport equation (see Sect. 6.1) in drag reduction. They use two-component laser velocimeter measurements in a fully developed turbulent channel flow to examine the effect of polymer injection on the Reynolds stresses and the production terms in the Reynolds stress transport equations. They determine that the production of the streamwise Reynolds normal stress was decreased, but production of the Reynolds shear stress was unchanged

showing that the processes represented by pressure–strain correlation terms in the Reynolds stress transport equations may be directly affected by the polymer.

2.2.3.2 Theoretical and Numerical Findings

At the same time as these developments were taking place, the effects of polymer extensibility and relaxation on the onset and the extent of drag reduction were investigated through rheological studies of drag-reducing polymers, Metzner and Park [61], Seyer and Metzner [62], Metzner [63], Bewersdorff and Berman [64]. However in spite of all these efforts, the fundamental mechanism which controls drag reduction has been elusive. The phenomenon is perplexing even today, and a satisfactory description is not yet at hand. No comprehensive understanding of the interaction of rheology and turbulence has ever been within our reach, much less a single theory capturing the main features of the drag reduction phenomenon. However, substantial progress has been made in the last decade in understanding the basic underlying physics as indicated by the recent reviews, Graham [65] and Wang et al. [66]. Even though some details are emerging and are better understood, the full picture is still not quite clear. Two of the prominent and competing ideas to explain Toms phenomenon have been formulated in the 1970s and are still under discussion. These are comparison and correlation of characteristic time scales and characteristic length scales. Lumley [67, 68] indicates that even though conceptually it maybe possible that an interaction between polymer molecules and hydrodynamic structure may occur because of corresponding length scales determined from polymer chain size and turbulent eddy size, it is unlikely that may be the dominant mechanism as the polymer length scale is too small, the ratio of the polymer length to eddy size being of order 10^{-2}. Consequently it is more appropriate to choose a characteristic time as a correlating parameter. It is believed that it is more likely that Toms phenomenon arises because of the characteristic relaxation time of polymer molecules becoming coupled or aligning itself somehow with the time-dependent flow of turbulent eddies in such a way that energy is stored rather than being dissipated, Schowalter [69], the difficulty with this idea being the lack of reliable information on characteristic relaxation times to characterize polydisperse solutions. In the strain energy storage model proposed by Kohn [70], polymer molecules store energy when they are strained by high-shear stress near the wall and release it by relaxation when transported to the low-shear region at the core. The onset of drag reduction occurs when strain energy convection is comparable to energy diffusion. Another idea central to attempts to explain drag reduction is the high resistance to extension of polymer solutions. It is assumed that this high resistance to stretching may inhibit vortex formation and that this may inhibit the continuous stretching of vortex filaments and their constant entwining and mixing with other filaments, thereby leading to a reduction in energy dissipation. In the 1990s significant evidence was obtained through numerical simulations using a generalized Newtonian model for dilute solutions that an enhanced, preferably anisotropic, extensional viscosity leads

to drag reduction in turbulent pipe flows, Toonder et al. [71], and turbulent channel flows, Orlandi [72]. Evidence from both numerical simulations and experiments points to reduced strength of the longitudinal vortices when long chain polymers are present in the flow. It is safe to say that up to this writing a vast majority of the proposed mechanisms of drag reduction are based on enhancing macromolecular resistance to extensional motions (high resistance to elongational strains) or elastic memory and relaxational effects. However, it is equally safe to state that the predictions of any theory put forth along these lines need improvement and direct uncontroversial evidence in support of any specific mechanism is still lacking.

The most promising tool that may have emerged starting with the mid-1990s is direct numerical simulation (DNS) due to advances made in numerical methods to resolve the structure of the boundary layer in the flow of dilute viscoelastic solutions and relate it to drag reduction. DNS has not only confirmed the established picture of wall-bounded turbulence but has also allowed a detailed evaluation of its structural and statistical features. The fully turbulent channel flow of a dilute polymer solution with the polymer chains modeled as finitely extensible elastic dumbbells based on the non-linear FENE-P model, which describes a polymer chain as two equal masses connected by a finitely extensible entropic spring (see Siginer [73] section 2.3.2.2), was investigated by Sureshkumar et al. [74] who used a direct numerical simulation (DNS) approach. The suitability of non-linear dumbbell models in describing the polymer conformation in *turbulent* flows was advocated earlier, Leal [75]. The simulation algorithm of Sureshkumar et al. [74] is based on a semi-implicit, time-splitting technique which uses spectral approximations in the spatial coordinates. The simulations show that the polymer induces several changes in the turbulent flow characteristics, all of them consistent with available experimental results. In particular, a decrease in the *rms* streamwise vorticity fluctuations and an increase in the average spacing between the streamwise streaks of low-speed fluid within the buffer layer were predicted (Fig. 2.3).

Since the quasi-streamwise vortices are known to play an important role in the production of turbulence, the observation of reduced *rms* streamwise vorticity seems to support a mechanism of drag reduction. These findings suggest a partial inhibition of turbulence generating events within the buffer layer by the macromolecules after the onset of drag reduction. They show that this inhibition is associated with an enhanced effective viscosity attributed to the extensional thickening properties of polymer solutions, previously proposed by Metzner, Lumley, and others. Using the simulation results obtained for different sets of parameter values which modify the relaxational and extensional properties of the model, a set of criteria for the onset of drag reduction is proposed. The existence of a critical Weissenberg number for the onset has been stipulated by several researchers in the past. For instance, based on their experiments Hershey and Zakin [76] proposed a transition Weissenberg number of $O(1)$ for fairly concentrated systems (>0.05 % by weight), but for a more dilute system (0.005 % by weight), a critical Weissenberg number $We_{cr} = 36$ was reported. Sureshkumar et al. [74] propose an onset Weissenberg number We_{cr} between 12.5 and 25 for dilute solutions based on simulations performed with the extensibility parameter $L = 10$ (L corresponds to the maximum

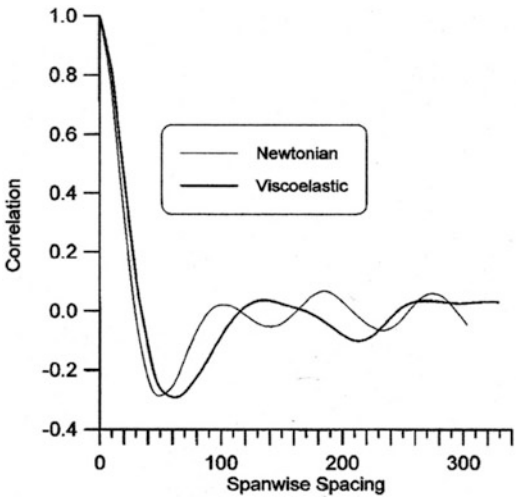

Fig. 2.3 The correlation of the streamwise fluctuating velocity as a function of spanwise spacing for both Newtonian and viscoelastic fluids (reprinted from Sureshkumar et al. [74] with permission)

value of the chain extension in the FENE-P model), which allows for sufficiently large extension of the polymer chains, contributing to an increased extensional viscosity. The Weissenberg number We_τ is defined as the product of the polymer relaxation time λ and a characteristic shear rate u_τ^2/ν_0 where ν_0 is the kinematic viscosity (diffusivity). u_τ is the friction velocity $u_\tau = \sqrt{\tau_w/\rho}$ where τ_w represents the shear stress at the wall and ρ is the density. Higher values of L indicate a high extensional viscosity and low values a low resistance to extensional strains. The maximum attainable extensional viscosity value is a monotonically increasing function of L for the FENE-P fluid; a high enough value of L is necessary to achieve significant drag reduction. Sureshkumar et al. [74] opt to use $L = 10$ in the computations after searching through a range of values for L. For instance, the mean flow velocity profiles obtained from the simulations performed for $L = 2$ at $We_\tau = 12.5$, 25, 37.5 and 50 are shown in Fig. 2.4 together with the Newtonian flow profile. All corresponding velocity profiles hardly deviate from Newtonian, and they all almost coincide indicating no detectable drag reduction for this low value of the elongational viscosity. For all the cases represented in Fig. 2.4, the root mean square velocity statistics are almost the same as the Newtonian flow results.

These observations are consistent with a mechanism for drag reduction requiring a significantly enhanced extensional viscosity in the bulk of the flow resulting in the suppression of the eddies which carry the Reynolds stress in the buffer layer, as proposed in the past by Lumley, Metzner, and others.

2.2.3.3 Factors Influencing the Effectiveness of Drag Reduction

Many factors have been identified that control the percent drag reduction with each drag-reducing additive.

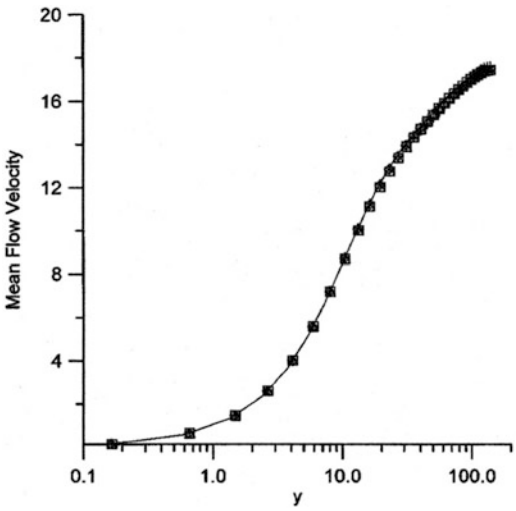

Fig. 2.4 The velocity $u(y)$ vs. y for the Newtonian (*solid line*) and four viscoelastic flows ($L = 2$) at $We = 12.5$ (*open diamond*), 25(+), 37.5 (*open square*), and 50 (*open triangle*) (reprinted from Sureshkumar et al. [74] with permission)

With fibers the effectiveness increases with fiber aspect ratio (length over diameter) and decreasing fiber diameter. Fibers mixed with polymers achieve drag reduction levels much higher than that for polymers or for fibers alone up to 95 %. An added advantage is that the polymer in a polymer fiber mixture is much less prone to degradation. With polymeric additives there are two well-established drag reduction types labeled type A and type B, Virk and Wagger [77]. Type A behavior occurs with very dilute solutions with which the onset of drag reduction at constant concentration only occurs in the fully turbulent regime above an onset Reynolds number. There is an onset shear stress and an onset shear rate. At Reynolds numbers less than the onset value, no drag reduction occurs. The onset may be due either to the stretching of the polymer molecules in the region of the flow field dominated by extension or to the entanglement of many molecules reaching the size of turbulent eddies. It is defined in terms of the onset shear stress or shear rate but not in terms of the onset Reynolds number because the latter is proportional to the 8/7th power of the pipe diameter, but the former is independent of it. The onset shear stress decreases with increasing molecular weight and radius of gyration of the polymer molecules, Virk [78]. Type B behavior happens with more concentrated polymer solutions. In this case the onset conditions can be reached at low Reynolds numbers. The laminar-turbulent transition is not observed, and laminar-like behavior is extended into an extended laminar region where drag reduction occurs. In both type A and type B behavior, drag reduction increases with flow rate until a critical wall shear stress is reached at which the rate of polymer degradation in the wall region exceeds the rate at which polymer is replenished in this region and drag reduction diminishes.

Other factors that influence the effectiveness of drag reduction are the molecular weight, the concentration effect, and the diameter effect. Polymers are generally ineffective for drag reduction if the molecular weight is less than 10^5, Hoyt

[79]. For a given concentration and Reynolds number, drag reduction increases with increasing average molecular weight, Virk [78]. Drag reduction at a fixed velocity increases with increasing polymer concentration until a saturation concentration is reached. Above this concentration, drag reduction starts falling off. The initial increase in drag reduction with increasing concentration is probably due to the increasing number of polymer molecules which cause the damping of a larger number of turbulent eddies. The decrease in drag reduction after the saturation concentration is caused by an increase in solution viscosity. With Newtonian fluids each Reynolds number in the turbulent region corresponds to a specific friction factor, which is independent of the tube diameter. In contrast at a given fixed Reynolds number, the same polymer solution in tubes of different diameter corresponds to different values of the friction factor. In general, the drag reduction observed in large pipes is smaller than that obtained in small pipe systems because of lower wall shear stresses and shear rates, Berman [80].

Surfactants are also effective drag reducers. In contrast to high polymers, their nanostructure can self-assemble after breakup by high shear, which makes them good candidates for use in recirculation systems containing high-shear pumps. Surfactant solutions are very sensitive to shear, which acts to induce reversible structural transformations in surfactant solutions manifesting themselves as shear thinning, shear-induced structures, shear-induced phase transitions (in shear bands), gelation, and flow instabilities, Fischer [81]. The mechanisms of these phenomena are not fully understood, although physical hypotheses and interpretation of the observed behavior have been formulated. For instance, it is thought that at low shear rates, surfactant solutions with rodlike or threadlike micelles usually act as Newtonian fluids because micelles rotate freely in the solution. At higher shear rates, micelles align themselves with the shearing direction causing shear thinning. Shear-induced structures occur at a critical shear rate at which the shear viscosity and elasticity show a sudden increase. These structures are orders of magnitude larger than the individual rodlike micelles, and the surfactant solution under these conditions behaves like a viscoelastic gel. The nature of shear-induced structures is not well understood in spite of considerable efforts. For instance, it is not known why it occurs with certain solutions and it does not with others.

In aqueous systems, when the critical surfactant concentration called the critical micelle concentration is reached, surfactant molecules gather into assemblies called micelles to minimize the hydrocarbon–water interface. When surfactant concentration is the same as or slightly above the critical micelle concentration, the shape of micelles is spherical or ellipsoidal. Micelles tend to form non-spherical shapes when the surfactant concentration reaches a second critical value. These shapes may be vesicles or disklike or may look like long cylinders called rodlike or wormlike micelles, which are generally considered excellent drag-reducing agents, Ohlendorf et al. [82]. The forces, which hold the surfactant molecules together in micelles, are much weaker than the primary chemical bonds of polymer molecules. But these forces persist even if the micelles encounter strong shear and breakup. They reform or self-assemble when the strong shear disappears, while polymer molecules cannot reform after mechanical degradation. The various factors that

influence and govern the drag-reducing ability of surfactants such as micelle shape and size and the effect of both critical surfactant concentrations together with the type of surfactant have been the subject of intense research in the last few decades, in particular in view of the suitability of surfactants for the district heating and cooling applications. The drag-reducing properties and the temperature operating range of non-ionic surfactants, which do not carry any charge; anionic surfactants, which are the only known effective surfactant drag reducers in hydrocarbon media; cationic surfactants, which are not easily biodegradable; and zwitterionic surfactants, the molecules of which carry both positive and negative charges on different locations of the molecules have been the subject of intense investigations. There is limited evidence that zwitterionic/anionic mixtures containing up to 20 % anionic are most effective drag reducers.

Scale-up studies to predict drag reduction performance in large pipes of practical flow systems from small diameter measurements in the laboratory are important for applications, Gasljevic et al. [83]. The drawback of surfactant use for drag reduction is a significant reduction, always a little larger than drag reduction, in the heat transfer ability of the surfactant solution, which happens in tandem with drag reduction and poses a problem when heat exchangers are in the loop, Aguilar et al. [84]. The underlining physical mechanism behind this behavior is not understood. However, remedies to enhance the heat transfer ability of the drag-reducing surfactant solutions have been proposed all of them centering essentially on breaking up the micelle nanostructure before the fluid enters the heat exchanger.

Research in drag reduction has stayed very active over the last several decades given the implications in applications, in particular in energy savings. Reviews by Berman [80], Virk [78], and White and Hemmings [85] in the 1970s; Hoyt [79] in 1985; the books by McComb [86] and Gyr and Bewersdorff [87, 88] in the 1990s; and the recent reviews by Graham [65] in 2004, White and Mungal [89] in 2008, and Wang et al. [66] in 2011 give excellent overviews of the state of the science up to the date of publication. Drag reduction in multiphase flows is a topic which deserves attention in its own right. It has been surveyed by Manfield et al. [90] in 1999, but not since then. Extensive bibliographies were given by Nadolink and Haigh [91] up to 1995 (4,900 publications related to drag reduction between 1922 and 1994) and by Ge [92] in 2008.

http://www.springer.com/978-3-319-02425-7

Developments in the Flow of Complex Fluids in Tubes

Siginer, D.A.

2015, X, 163 p. 31 illus., 3 illus. in color., Hardcover
ISBN: 978-3-319-02425-7